Supporting Information

In situ O_2-emission assisted synthesis of molybdenum carbide nanomaterials as an efficient electrocatalyst for hydrogen production in both acidic and alkaline media

Lvlv Ji, Jianying Wang, Lixia Guo and Zuofeng Chen*

Shanghai Key Lab of Chemical Assessment and Sustainability, School of Chemical Science and Engineering, Tongji University, Shanghai 200092, China

EXPERIMENTAL

Materials. Aniline (99.5%), phosphomolybdic acid (AR), hydrogen peroxide (30 wt%), ammonium persulfate (98%) and sodium chloride (AR) were purchased from Sigma-Aldrich Co. 20 wt% Pt/C was purchased from Alfa Aesar Chemical Reagent Co. Sulfuric acid (98%), hydrochloric acid (37.5%) and *N,N*-dimethylformamide (>99.9%, GC) were purchased from Energy Chemical Reagent Co. High-purity air and argon (99.999%) gases were purchased from Shanghai Gases Co. Prior to its use, aniline was purified by redistillation. All other chemical reagents were of analytical grade and used as received without further purification.

Apparatuses. FT-IR spectra were obtained on a Nicolet 6700 spectrometer (Thermo Fisher Nicolet, USA) with KBr pellets. Raman spectra were recorded on a confocal

*Corresponding author

E-mail address: zfchen@tongji.edu.cn (Z.-F. Chen)

microscope laser Raman spectrometer (Rainshaw invia). UV-vis absorption spectra in wavelength between 300 - 800 nm were recorded on a SPECORD® 200 PLUS (Analytikjena, Germany) diode-array spectrophotometer. *N,N*-Dimethylformamide (DMF) solvent was used to dissolve the polymer.

Scanning electron microscope (SEM) images and energy dispersive X-ray analysis (EDX) data were obtained at Hitachi S-4800 (Hitachi, Japan) equipped with a Horiba EDX system (X-max, silicon drift X-Ray detector). SEM images were obtained with an acceleration voltage of 3 kV and EDX spectra were obtained with an acceleration voltage of 15 kV. Transmission electron microscopy (TEM) images, high resolution TEM (HRTEM) images and selected area electron diffraction (SAED) patterns were obtained using JEM-2100, JEOL.

Powder X-ray diffraction (XRD) was measured by Bruker Foucs D8 *via* ceramic monochromatized Cu Kα radiation of 1.54178 Å, operating at 40 kV and 40 mA. The scanning rate was 5° per min in 2θ and the scanning range was from 10 - 80°.

X-ray photoelectron spectroscopy (XPS) for elemental analysis was conducted on a Kratos Axis Ultra DLD X-ray Photoelectron Spectrometer using 60 W monochromated Mg Kα radiation as the X-ray source for excitation. The 500 μm X-ray spot was used for XPS analysis. The base pressure in the analysis chamber was about 3×10^{-10} mbar. The carbon 1s peak (284.6 eV) was used for internal calibration. The peak resolution and fitting were processed with the XPS Peak 41 software.

The Brunauer-Emmett-Teller (BET) surface areas of the samples were measured on a Quanta Chrome Nova 2200e by nitrogen adsorption at 77.4 K. The samples were degassed

for 3 h at 300 °C prior to measurements.

Thermogravimetric analysis (TGA) measurements of Mo_xC@NPC materials were conducted on a TGA Q500 at temperatures from 25 to 650 °C with a ramping rate of 10 °C min^{-1} under the high-purity air atmosphere. For CN, the temperature was increased from 25 to 1000 °C with the same ramping rate under the air atmosphere. An additional TGA measurement of Mo_2C@NPC-4 was further conducted at temperatures from 25 to 1300 °C with the same ramping rate but under the nitrogen atmosphere.

Electrochemical measurements were performed on a CHI 660E electrochemical workstation (Chenhua Corp., Shanghai, China).

Synthesis of PANI nanofibers. The synthesis of polyaniline (PANI) nanofibers follows the literature procedure.[1] Briefly, 2 ml aniline (ANI, 0.021 mol) was dissolved in 100 ml aqueous 1 M HCl/saturated NaCl solution with a magnetically stirring, followed by addition of 5 ml 30 wt% H_2O_2. The reaction mixture was heated to 60 °C on a hot plate for 10 min with stirring, and it was then cooled down to room temperature (about 25 °C) naturally. After that, the reaction was proceeding for another 2 h. The powders were collected by filtering the resultant suspension, then washing with deionized water and acetone until the filtrate was colorless. The obtained PANI nanofibers was dried in the vacuum oven at 60 °C for 24 h.

Synthesis of PANI-PMo_{12} polymeric hybrids. In a typical synthesis, 4 g phosphomolybdic acid (PMo_{12}, 2.2 mmol) was first dissolved in 100 ml aqueous 1 M HCl/saturated NaCl solution with a magnetically stirring. 2 ml ANI (0.021 mol) was then added and the solution turned pale yellow due to the formation of the aniline

heteropolyacid salt, in which 5 ml H_2O_2 (30 wt%) was subsequently added. The reaction mixture was heated to 60 ^oC on a hot plate for 10 min with stirring, and it was then cooled down to room temperature (about 25 ^oC) naturally. The color of the reaction solution gradually turned black accompanied with lots of O_2 bubbles produced in the solution. The reaction was then proceeding for another 2 h. The products were separated by filtration and washed with deionized water and acetone until the filtrate was colorless. At this stage, PANI was doped with PMo_{12} anions and Cl^- from HCl and NaCl. Cl^- contamination was eliminated *via* an ion-exchange method followed by washing with deionized water.[2] In this process of ion-exchange, 0.5 g PMo_{12} was dissolved in 100 ml water, in which the resultant products were added. The solution mixture was stirred at the room temperature for 24 h. The final dark brown powders (denoted as PANI-PMo_{12}-4) were obtained by filtering, washing with deionized water until the filtrate was colorless, and drying in the vacuum oven at 60 ^oC for 24 h. In the parallel experiments, PANI-PMo_{12}-1, PANI-PMo_{12}-2 and PANI-PMo_{12}-6 were synthesized under identical conditions except that the amounts of feeding PMo_{12} during the polymerization were 1, 2 and 6 g, and the amounts of PMo_{12} used for the ion-exchange purification were 0.125, 0.25 and 0.75 g.

As a control experiment, PANI-PMo_{12} hybrid was also synthesized with ammonium persulfate (APS) as the polymerization oxidant. Specifically, 4 g PMo_{12} were dissolved in 100 ml aqueous 1 M HCl solution with a magnetically stirring and then 2 ml ANI was added to form the aniline heteropolyacid salt. Afterwards, 5 ml aqueous APS solution (30 wt%) was dropwise added within 5 min. The reaction was then proceeding for another 16 h and the color of the solution mixture turned black gradually with no bubbles observed.

The products were separated by filtration and washed with deionized water and acetone until the filtrate was colorless. To remove the Cl^- contamination, the same ion-exchange method was applied in PMo_{12} (0.5 g) aqueous solution. The final dark green powders (denoted as PANI-PMo_{12}-4/APS) were collected by filtering, washing with deionized water until the filtrate was colorless, and drying in the vacuum oven at 60 ^oC for 24 h.

Synthesis of pyrolyzed CN and Mo_xC@NPC electrocatalysts. CN was prepared by pyrolyzing PANI nanofibers under argon atmosphere at 900 ^oC for 2 h with a temperature ramp of 5 ^oC min^{-1}. The Mo_xC@NPC series samples were obtained by pyrolyzing the PANI-PMo_{12} polymeric hybrids by the same procedure. The pyrolyzed samples were acid-etched in 0.5 M H_2SO_4 solution for 24 h at 80 ^oC by oil-bath heating to get rid of inactive and unstable species. Finally, the acid-etched samples were washed with deionized water thoroughly until the eluent reaching a neutral pH. The final products were defined as MoC@NPC-1, MoC@NPC-2, Mo_2C@NPC-4 and Mo_2C@NPC-6, respectively, according to the initial feeding content of PMo_{12}.

A contrast sample Mo_2C@NPC-4/APS with the precursor prepared using APS as the polymerization oxidant, was obtained by the same pyrolysis and acid-etching procedure.

Electrochemical measurements. To prepare the working electrode, a total of 4 mg of the electrocatalyst and 80 μl of 5 wt% Nafion solution were dispersed in 1 ml of 4:1 (v/v) water/ethanol by 30 min sonication. Five microliters of the electrocatalyst suspension were dropped onto the glassy carbon electrode (mass loading ~ 0.265 mg cm^{-2}), which was allowed to dry at 50 ^oC for 30 min in the oven. The three-electrode system consisted of a working electrode, a Pt coiled wire counter electrode, and a saturated calomel

reference electrode (SCE). The potentials reported were referred to the Reversible Hydrogen Electrode (RHE) *via* the Nernst equation: $E_{RHE} = E_{SCE} + 0.059pH + 0.244$. In 0.5 M H_2SO_4, $E_{RHE} = 0.273\ V + E_{SCE}$; in 1 M NaOH, $E_{RHE} = 1.05\ V + E_{SCE}$. Unless stated otherwise, linear sweep voltammetry (LSV) was conducted with a scan rate of 2 mV s^{-1}. The Tafel slope was obtained from the LSV plot using a linear fit applied to points in the Tafel region. Electrochemical impedance spectroscopy (EIS) measurements were carried out from 100 kHz to 100 mHz with an amplitude of 5 mV at the open-circuit voltage. The electrochemical stability of the catalyst was conducted by cycling the potential between -0.2 and 0.2 V *vs* RHE at a scan rate of 100 mV s^{-1}. Additionally, the long-term electrolysis was measured at an overpotential of 150 mV for 10 h in both 0.5 M H_2SO_4 and 1 M NaOH. The electrolyte solution was degassed for 10 min by nitrogen to remove the dissolved oxygen, and a flow of nitrogen gas was maintained above the electrolyte solution during the electrochemical experiments. LSV and Tafel data plots were corrected by the ohmic drop based on the EIS measurement. The experiments were all performed at 22 ± 2 °C.

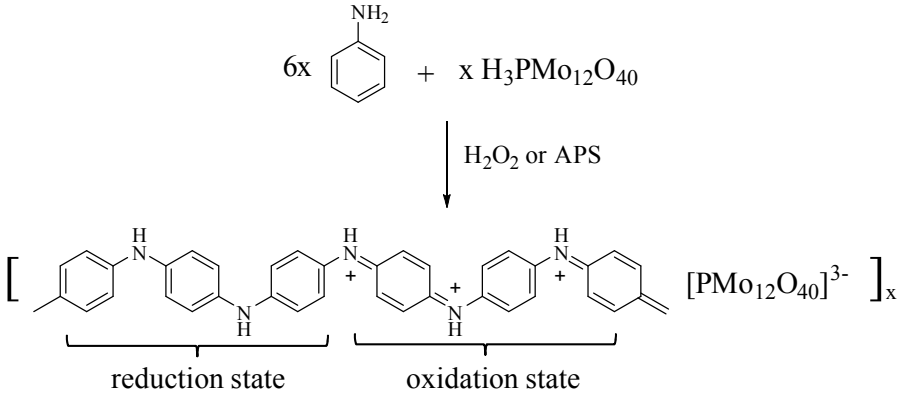

Scheme S1. Synthesis of PANI doped with PMo_{12} anions.[3]

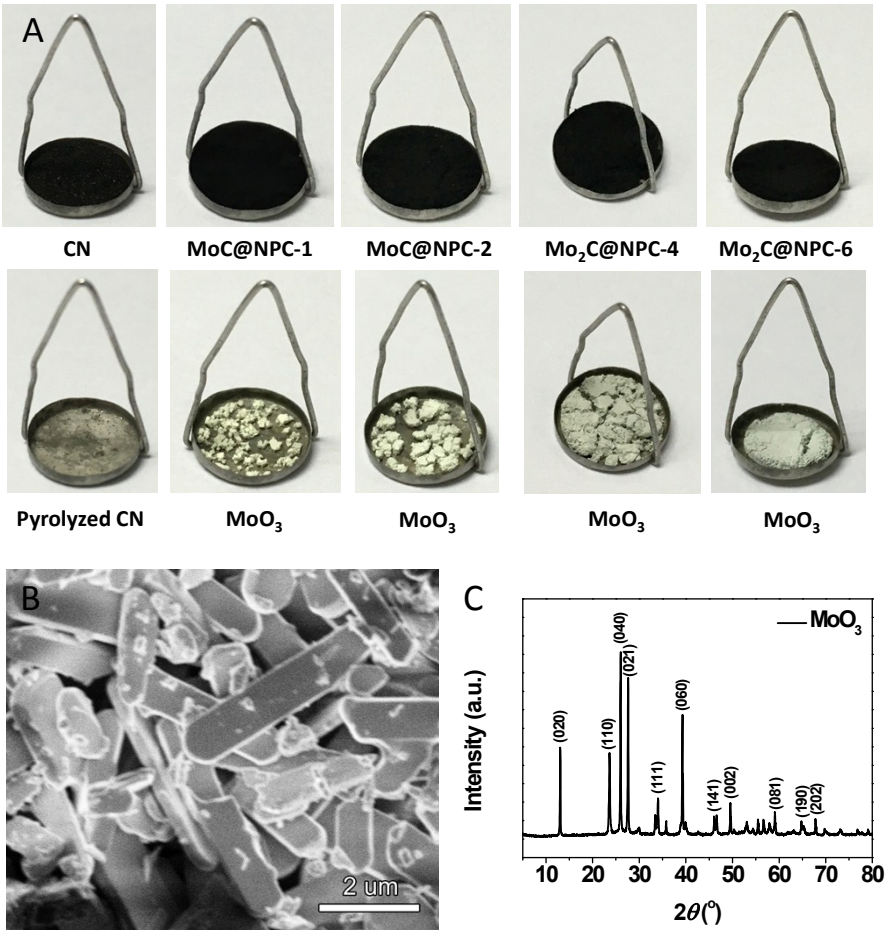

Figure S1. (A) Digital camera pictures of CN, MoC@NPC-1, MoC@NPC-2, Mo_2C@NPC-4 and Mo_2C@NPC-6 before and after TGA measurements under air atmosphere. (B) SEM image and (C) XRD pattern of MoO_3 nanobelts obtained from Mo_xC@NPC materials after TGA measurements under air atmosphere.

To determine Mo content from TGA curves, we assume that the samples consist of only stoichiometric Mo_xC and carbon, and after heating to 650 ^oC, all Mo_xC have been totally converted to MoO_3 and all the carbon-based materials have been completely burned. Therefore, the carbon content is estimated according to the following equations:

(1) $m_{carbon}\% = 100\% - m_{MoC}\% = 100\% - m_{residual\ mass}\% \times M(MoC) / M(MoO_3)$;

(2) $m_{carbon}\% = 100\% - m_{Mo2C}\% = 100\% - m_{residual\ mass}\% \times M(Mo_2C) / (2 \times M(MoO_3))$.

For MoC@NPC-1, m_{MoC}% = (36.5% × 108) / 144 = 27.4% and m_{carbon}% = 72.6%. The atomic percentage of Mo is calculated to be 3.9 at%.

For MoC@NPC-2, m_{MoC}% = (52.9% × 108) / 144 = 39.7% and m_{carbon}% = 60.3%. The atomic percentage of Mo is calculated to be 6.4 at%.

For Mo_2C@NPC-4, m_{Mo2C}% = (70.4% × 204) / (2 × 144) = 49.9% and m_{carbon}% = 50.1%. The atomic percentage of Mo is calculated to be 10 at%.

For Mo_2C@NPC-6, m_{Mo2C}% = (81.3% × 204) / (2 × 144) = 57.6% and m_{carbon}% = 42.4%. The atomic percentage of Mo is calculated to be 12.9 at%.

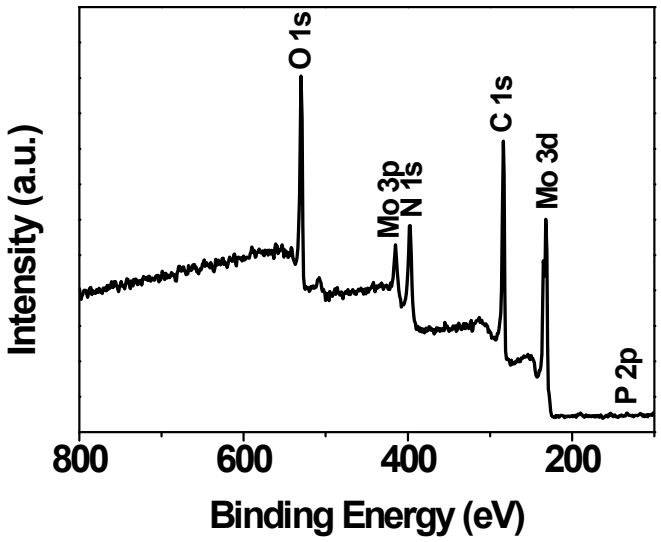

Figure S2. XPS survey spectrum of Mo_2C@NPC-4.

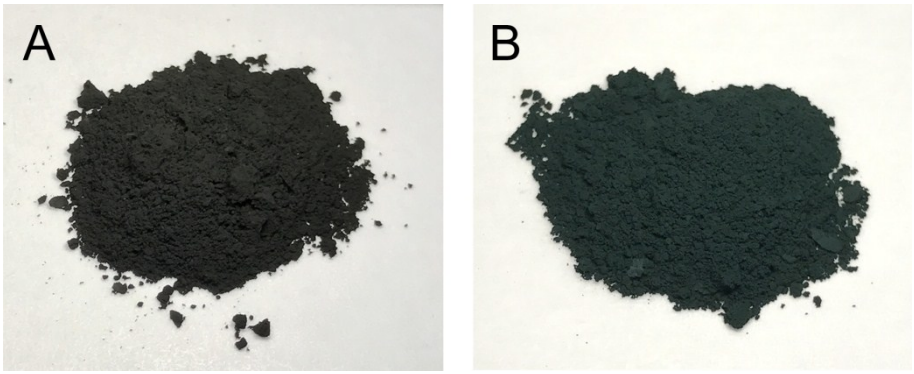

Figure S3. Digital camera pictures of PANI-PMo_{12}-4 (A) and PANI-PMo_{12}-4/APS (B). As can be seen, PANI-PMo_{12}-4 is dark brown, and PANI-PMo_{12}-4/APS is dark green.

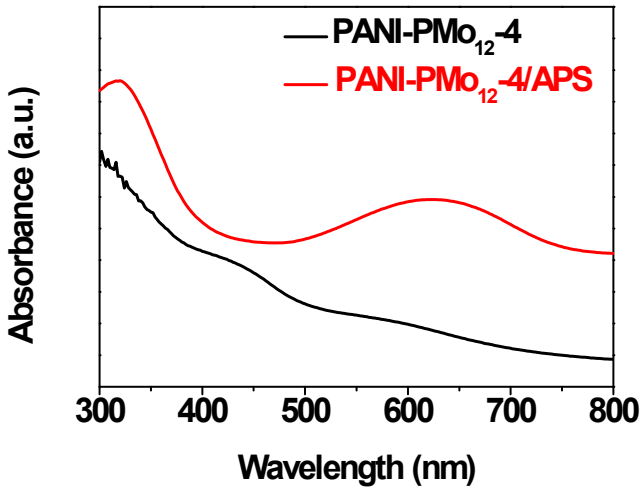

Figure S4. UV-vis absorption spectra of PANI-PMo_{12}-4 and PANI-PMo_{12}-4/APS dissolved in DMF.

The ratio of quinonoid imine/benzenoid amine is an indicator of the intrinsic oxidation state of PANI. As can be seen, PANI-PMo_{12}-4/APS shows two broad absorption bands centered at 320 and 624 nm, attributed to π-π^* transition in the benzenoid amine unit and n-π^* transition in the quinonoid imine unit, respectively.[4] In PANI-PMo_{12}-4, the intensity of the absorption at 624 nm is greatly decreased, indicating the presence of a much smaller fraction of quinonoid imine groups in this sample.[4] Therefore, PANI-PMo_{12}-4/APS (*i.e.*

PANI in the hybrid) bears a higher intrinsic oxidation state than PANI-PMo_{12}-4, which explains the different powders colors in Figure S3. This observation is consistent with the fact that APS is a stronger oxidant than H_2O_2. The polymeric hybrid with a higher intrinsic oxidation state can attract more PMo_{12} anions during polymerization, leading to a higher Mo loading in Mo_2C@NPC-4/APS.

The barely discernable peak at 450 nm is due to the transition from polaron band to π* band, which represents the delocalized polaron intrachain transition.[5,6]

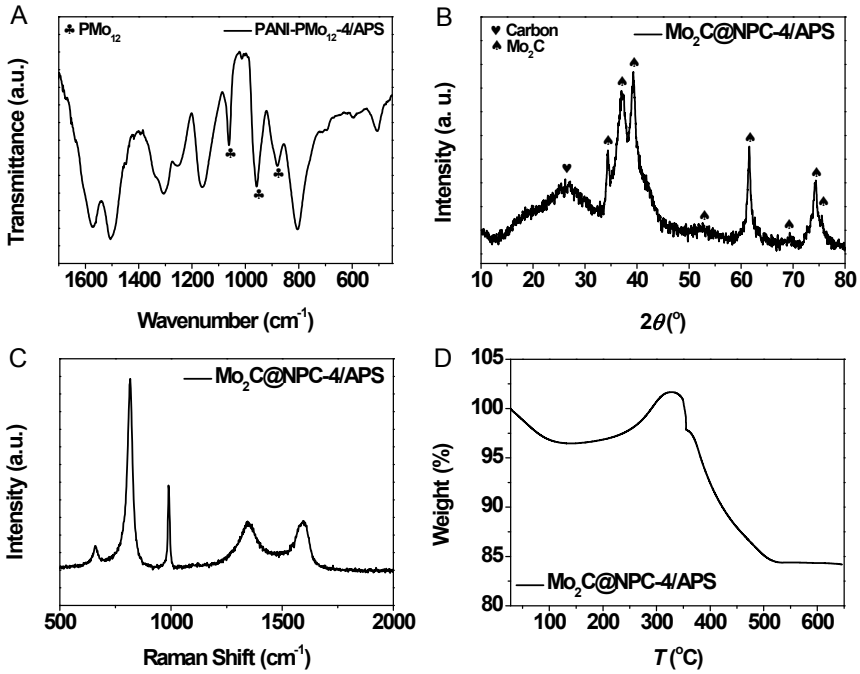

Figure S5. (A) FT-IR spectrum of PANI-PMo_{12}-4/APS. (B) XRD pattern, (C) Raman spectrum and (D) TGA curve of Mo_2C@NPC-4/APS. TGA measurement was conducted under air atmosphere.

In (A), the absorption peaks located at 1064, 954 and 897 cm^{-1} are attributable to PMo_{12}, while other peaks are assigned to PANI.

In (B), the diffraction peak at 26° is indexed to the amorphous carbon-based material and other diffraction peaks located at approximately 34.3°, 37.3°, 39.1°, 52°, 61.5°, 69.5°,

74.4° and 75.4° are assigned to Mo_2C (PDF#35-0787).

In (C), the two Raman peaks located at around 1342 and 1595 cm^{-1} are attributed to the D-band and G-band of the carbon-based material, and the other three Raman peaks located at around 657, 816 and 992 cm^{-1} are attributable to Mo_2C.

In (D), the initial weight loss below 200 °C is due to the loss of the residual water. The gradual oxidation of Mo_2C to MoO_3 occurs above 200 °C, leading to a slight weight gain, which is followed by a significant weight loss above 340 °C due to the carbon combustion.

Similar to the treatment in Figure S1, the atomic percentage of Mo can be calculated for Mo_2C@NPC-4/APS: $m_{Mo2C}\%$ = (84.2% × 204) / (2 × 144) = 59.6% and $m_{carbon}\%$ = 40.4%. The atomic percentage of Mo is calculated to be 13.8 at%.

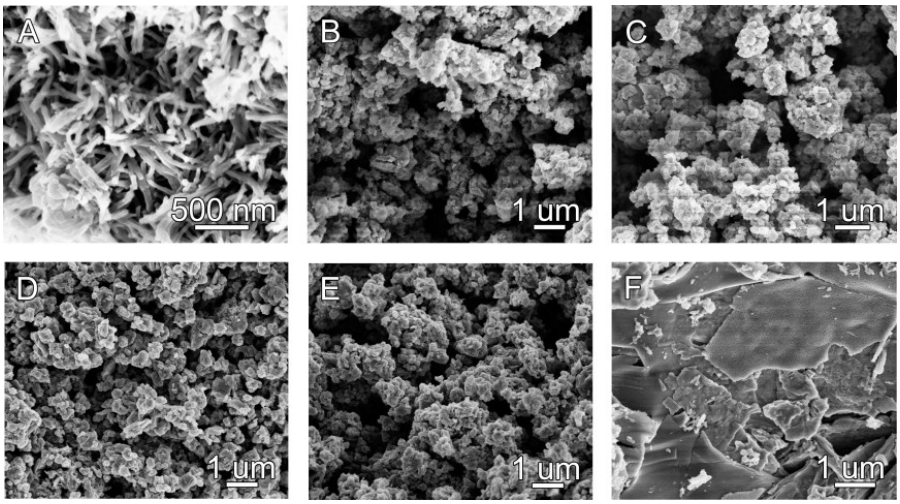

Figure S6. SEM images of (A) PANI nanofibers, (B) PANI-PMo_{12}-1, (C) PANI-PMo_{12}-2, (D) PANI-PMo_{12}-4, (E) PANI-PMo_{12}-6 and (F) PANI-PMo_{12}-4/APS.

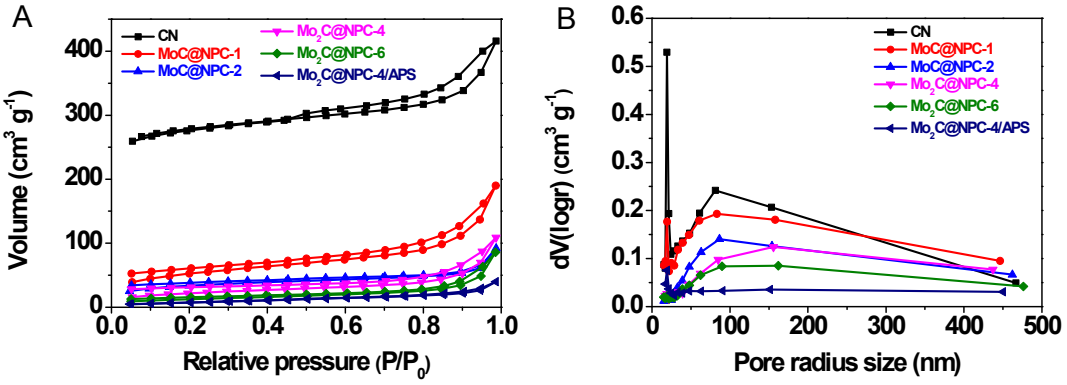

Figure S7. (A) N_2 adsorption/desorption isotherms and (B) pore size distributions of CN, MoC@NPC-1, MoC@NPC-2, Mo_2C@NPC-4, Mo_2C@NPC-6 and Mo_2C@NPC-4/APS.

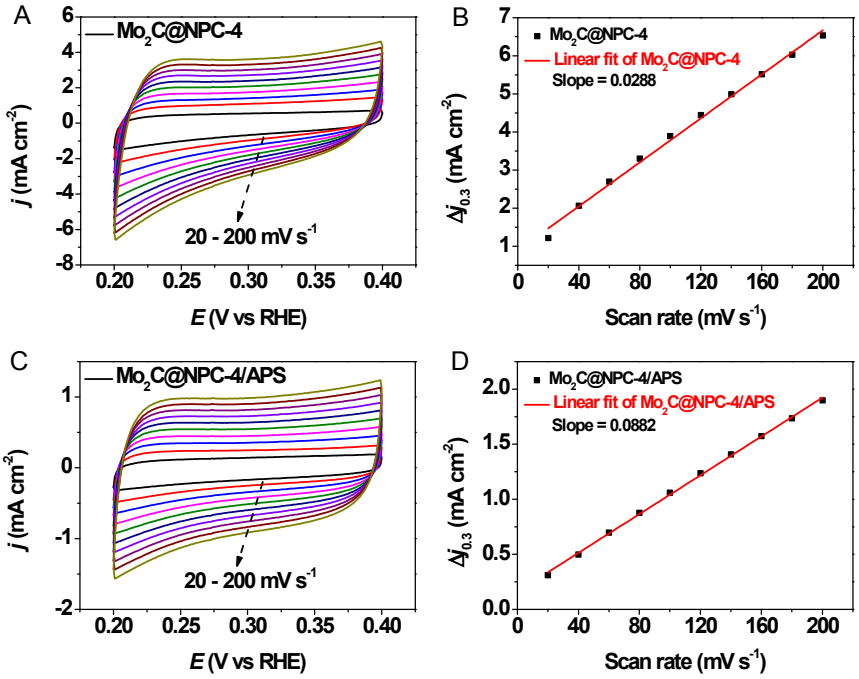

Figure S8. CVs of (A) Mo_2C@NPC-4 and (C) Mo_2C@NPC-4/APS with different scan rates from 20 to 200 mV s^{-1} under the potential window of 0.2 – 0.4 V vs RHE; the capacitive current at 0.3 V as a function of scan rate for (B) Mo_2C@NPC-4 and (D) Mo_2C@NPC-4/APS.

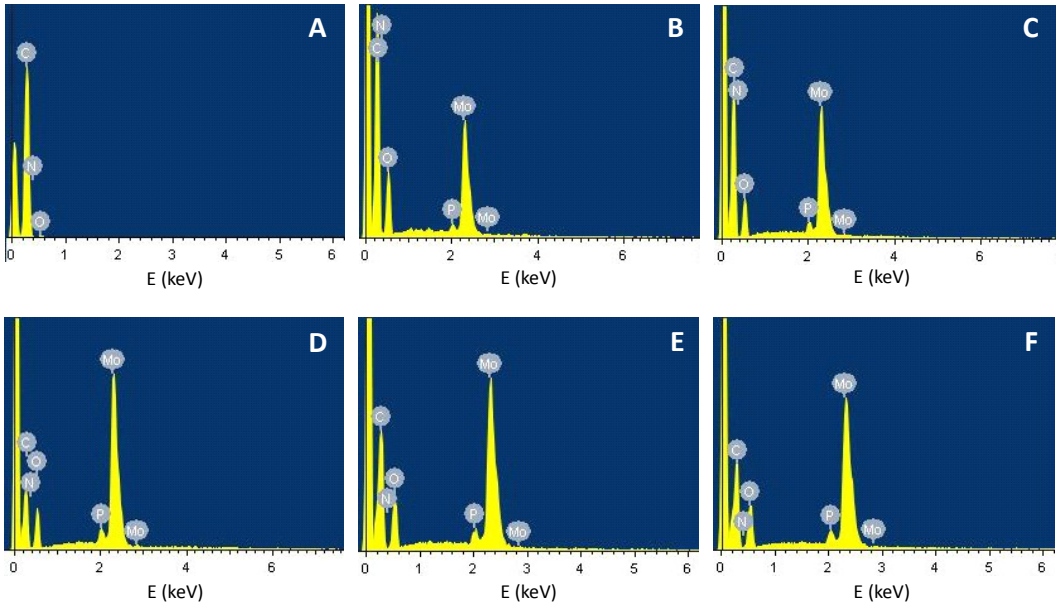

Figure S9. SEM-EDX spectra of (A) CN, (B) MoC@NPC-1, (C) MoC@NPC-2, (D) Mo_2C@NPC-4, (E) Mo_2C@NPC-6 and (F) Mo_2C@NPC-4/APS.

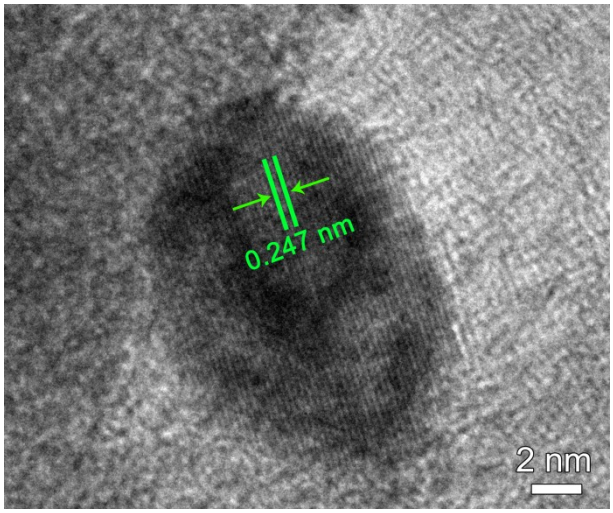

Figure S10. HRTEM image of MoC@NPC-1.

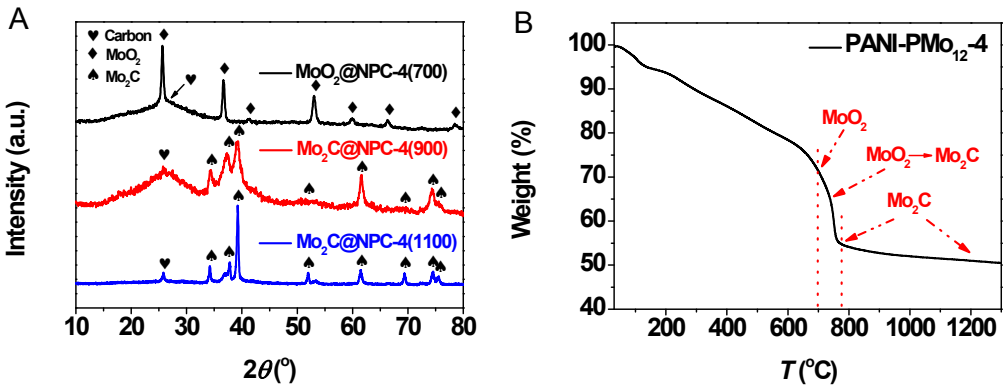

Figure S11. (A) XRD patterns of MoO_2@NPC-4(700), Mo_2C@NPC-4(900) and Mo_2C@NPC-4(1100). (B) TGA curve of PANI-PMo_{12}-4 under nitrogen atmosphere.

In (A), the XRD pattern of MoO_2@NPC-4(700) indicates a typical MoO_2 structure with characteristic peaks located at approximately 25.6°, 36.6°, 41°, 53°, 59.6°, 66.3° and 78.5° (PDF#76-1807).[7] By contrast, the XRD patterns of Mo_2C@NPC-4(900) and Mo_2C@NPC-4(1100) indicate a typical Mo_2C structure. The XRD pattern of Mo_2C@NPC-4(1100) exhibit sharper diffraction peaks, indicating formation of highly crystalline Mo_2C particles at the higher temperature. The peak at around 26° is observed for all three samples, which is attributed to the amorphous carbon residues.

In (B), TGA curve of PANI-PMo_{12}-4 under nitrogen atmosphere is recorded. The initial weight loss below 150 °C is due to the loss of the residual water, and the gradual weight loss between 150 °C and 700 °C is attributable to the decomposition and carbonation of the polymer chain, as well as the transformation from PMo_{12} to MoO_2. A sharp weight loss was observed between 700 °C and 780 °C which can be attributed to the formation of Mo_2C phase from MoO_2 and carbon matrix. Beyond 780 °C, the gradual weight loss is attributed to the gradual burning of residual polymer and N and P element.[8]

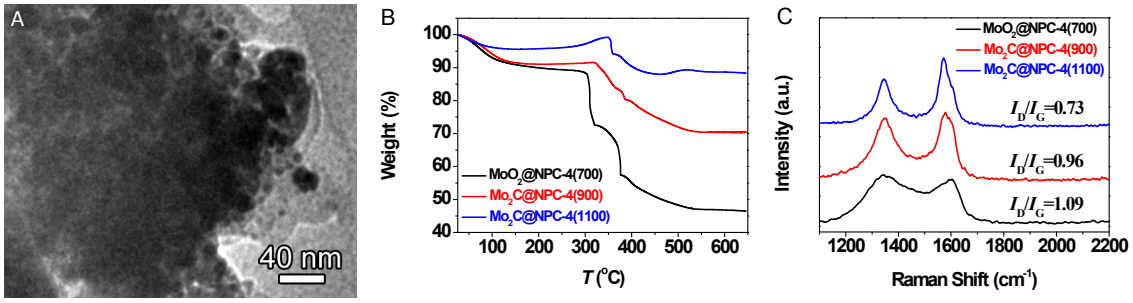

Figure S12. (A) TEM image of Mo_2C@NPC-4(1100). (B) TGA curves of MoO_2@NPC-4(700), Mo_2C@NPC-4(900) and Mo_2C@NPC-4(1100) under air atmosphere. (C) Raman spectra of MoO_2@NPC-4(700), Mo_2C@NPC-4(900) and Mo_2C@NPC-4(1100).

In (A), the TEM image shows that the Mo_2C@NPC-4(1100) samples prepared at 1100 ^oC experience severe aggregation of Mo_2C nanoparticles.

In (B), TGA curves of MoO_2@NPC-4(700), Mo_2C@NPC-4(900) and Mo_2C@NPC-4(1100) are recorded under high-purity air atmosphere. Similar to the treatment in Figure S1, the atomic percentage of Mo can be calculated for MoO_2@NPC-4(700) and Mo_2C@NPC-4(1100):

For MoO_2@NPC-4(700), $m_{MoO2}\%$ = (46.4% × 128) / 144 = 41.2% and $m_{carbon}\%$ = 58.8%. The atomic percentage of Mo is calculated to be 5.5 at%.

For Mo_2C@NPC-4(1100), $m_{Mo2C}\%$ = (88.3% × 204) / (2 × 144) = 62.5% and $m_{carbon}\%$ = 37.5%. The atomic percentage of Mo is calculated to be 15.2 at%.

In (C), for MoO_2@NPC-4(700), two distinct peaks are observed at around 1342 and 1602.5 cm^{-1} attributed to the D-band and G-band of the carbon-based materials. For Mo_2C@NPC-4(900) and Mo_2C@NPC-4(1100), the G-band peak has been slightly moved to 1578.7 and 1571.1 cm^{-1}, respectively, which may be related to the structure and valence change of carbon with different amount of N and P doping. For the Raman spectra, the D-

band and G-band correspond to the disordered graphitic carbon and graphite carbon, respectively. The I_D/I_G peak intensity ratios obtained for MoO_2@NPC-4(700), Mo_2C@NPC-4(900) and Mo_2C@NPC-4(1100) are 1.09, 0.96 and 0.73, respectively, indicating that the contents of N and P dopants decrease with increasing the pyrolysis temperature.

Table S1. Mo and C contents in various pyrolyzed samples determined by TGA analysis[a].

Sample	Mo content (at%)	C content (at%)
MoC@NPC-1	3.9	96.1
MoC@NPC-2	6.4	93.6
Mo_2C@NPC-4	10	90
Mo_2C@NPC-6	12.9	87.1
Mo_2C@NPC-4/APS	13.8	86.2
MoO_2@NPC-4(700)	5.5	94.5
Mo_2C@NPC-4(1100)	15.2	84.8

[a] Only C and Mo elements are taken into account for the calculation.

Table S2 The specific surface area and the total pore volume of the as-prepared

electrocatalysts.

Sample	A_{BET} (m^2 g^{-1})	Total pore volume (cm^3 g^{-1})
CN	922	0.643
MoC@NPC-1	190.8	0.294
MoC@NPC-2	121.6	0.205
Mo_2C@NPC-4	79.3	0.168
Mo_2C@NPC-6	45.9	0.133
Mo_2C@NPC-4/APS	28.3	0.062

Table S3. Element contents in the as-prepared electrocatalysts determined by EDX

analysis.

Sample	C %	N %	O %	P %	Mo %
CN	92.27	4.8	2.93	0	0
MoC@NPC-1	79.42	4.13	13.7	0.13	2.62
MoC@NPC-2	75.99	3.97	16.07	0.23	3.74
Mo_2C@NPC-4	69.38	3.68	19.06	0.44	7.44
Mo_2C@NPC-6	65	3.45	21.3	0.57	9.68
Mo_2C@NPC-4/APS	62.39	3.17	22.95	0.65	10.84
MoO_2@NPC-4(700)	68.03	5.62	22.03	0.87	3.45
Mo_2C@NPC-4(1100)	70.09	2.83	15.19	0.26	11.63

Table S4. Comparison of the HER activity of the as-prepared electrocatalysts in 0.5 M H_2SO_4.

Electrocatalyst	j (mA cm^{-2})	η (mV)	b (mV dec^{-1})
CN	10	470	223
MoC@NPC-1	10	309	118
MoC@NPC-2	10	240	75.3
Mo_2C@NPC-4	10	152	52.5
Mo_2C@NPC-6	10	173	56.8
Mo_2C@NPC-4/APS	10	205	62.1
MoO_2@NPC-4(700)	10	621	133
Mo_2C@NPC-4(1100)	10	216	67

Table S5. Comparison of the HER activity of Mo_2C@NPC-4 with the reported Mo_xC-based electrocatalysts in acidic solution.

Electrocatalyst	j (mA cm^{-2})	η (mV)	b (mV dec^{-1})	Electrolyte solution	Ref.
Mo_2C@NPC-4	10	144	52.5	0.5 M H_2SO_4	this work
Mo_2C@NPC/NPRGO	10	34	33.6	0.5 M H_2SO_4	8
np-Mo_2C NWs	10	130	53	0.5 M H_2SO_4	9
Mo_2C/CNT	10	152	55.2	0.1 M $HClO_4$	10
Mo_2C/GCSs	10	200	62.6	0.5 M H_2SO_4	11
Mo_2C/CNT-GR	10	130	58	0.5 M H_2SO_4	12
MoC_x nano-octahedrons	10	142	53	0.5 M H_2SO_4	13
Mo_2C-G	10	130	57	0.5 M H_2SO_4	14
PDAP-MoCN-CO_2	10	140	46	H_2SO_4 (pH=1)	15
MoDCA-5	10	78	41	0.5 M H_2SO_4	16
MoC_x@C-1	10	79	56	0.5 M H_2SO_4	17
Mo_2C@NC	10	124	60	0.5 M H_2SO_4	18
Mo_2C-NCNTs	10	147	71	0.5 M H_2SO_4	19
Mo_1Soy/RGO	10	109	62.7	0.5 M H_2SO_4	20
β-Mo_2C nanotube	10	172	62	0.5 M H_2SO_4	21
Mo_2C-R	10	150	58	0.5 M H_2SO_4	22
Co-Mo_2C-0.020	10	140	39	0.5 M H_2SO_4	23

Table S6. Comparison of the HER activity of the as-prepared electrocatalysts in 1 M NaOH.

Electrocatalyst	j (mA cm^{-2})	η (mV)	b (mV dec^{-1})
CN	10	512	116
MoC@NPC-1	10	293	90.9
MoC@NPC-2	10	255	78.8
Mo_2C@NPC-4	10	141	47.5
Mo_2C@NPC-6	10	180	55.4
Mo_2C@NPC-4/APS	10	213	63.8
MoO_2@NPC-4(700)	10	719	156.5
Mo_2C@NPC-4(1100)	10	232	69.4

Table S7. Comparison of the HER activity of Mo_2C@NPC-4 with the reported Mo_xC-based electrocatalysts and some noble-metal-free electrocatalysts in basic solution.

Electrocatalyst	j (mA cm^{-2})	η (mV)	b (mV dec^{-1})	Electrolyte solution	Ref.
Mo_2C@NPC-4	10	141	47.5	1 M NaOH	this work
MoC_x nano-octahedrons	10	151	62.6	1 M KOH	13
Mo_2C@NC	10	60	/	1 M KOH	18
Mo_2C-NCNTs	10	257	/	1 M KOH	19
30wt%Ni-Mo_2C-R	10	130	49	1 M KOH	22
Mo_2C nanoparticles	10	176	58	1 M KOH	24
Mo_2C	10	190	54	1 M KOH	25
Mo_2B	10	220	59	1 M KOH	25
WC-1050	10	137	106	0.1 M KOH	26
CoP/CC	10	209	129	1 M KOH	27
FeP NAs/CC	10	218	146	1 M KOH	28
0.27Mo2.4Ni@800	10	126	93	1 M KOH	29
N-Co@G	10	337	/	0.1 M NaOH	30
WN NA/CC	10	285	170	1 M KOH	31
Co-NRCNTs	10	370	/	1 M KOH	32
NiS_2 NA/CC	10	149	104	1 M KOH	33
Ni_2P NS/CC	10	102	65	1 M KOH	34
N,P-graphene-1	1	500	145	0.1 M KOH	35

Description of Supplementary Movie 1

Two sample bottles were filled with 5 ml 20 mM PMo_{12}/1 M HCl solution. Afterwards, 1 ml aqueous APS solution (30 wt%) was added into the left bottle and 1 ml H_2O_2 (30 wt%) was added into the right bottle. As can been seen, vigorous gas bubbles were generated in the right bottle due to H_2O_2 decomposition catalyzed by PMo_{12} while no bubbles were generated in the left bottle.

Supplementary references

1 S. P. Surwade, S. R. Agnihotra, V. Dua, N. Manohar, S. Jain, S. Ammu and S. K. Manohar, *J. Am. Chem. Soc.*, 2009, **131**, 12528-12529.

2 H. Yang, T. Song, L. Liu, A. Devadoss, F. Xia, H. Han, H. Park, W. Sigmund, K. Kwon and U. Paik, *J. Phys. Chem. C*, 2013, **117**, 17376-17381.

3 M. Lira-Cantú and P. Gómez-Romero, *Chem. Mater.*, 1998, **10**, 698-704.

4 E. T. Kang, K. G. Neoh and K. L. Tan, *Prog. Polym. Sci.*, 1998, **23**, 277-324.

5 Y. Xia, J. M. Wiesinger, A. G. MacDiarmid and A. J. Epstein, *Chem. Mater.*, 1995, **7**, 443-445.

6 Y. F. Nicolau, P. M. Beadle and E. Banka, Syn. Met., 1997, **84**, 585-586.

7 Y. J. Tang, M. R. Gao, C. H. Liu, S. L. Li, H. L. Jiang, Y. Q. Lan, M. Han and S. H. Yu, *Angew. Chem. Int. Ed.*, 2015, **54**, 12928-12932.

8 J. S. Li, Y. Wang, C. H. Liu, S. L. Li, Y. G. Wang, L. Z. Dong, Z. H. Dai, Y. F. Li and Y. Q. Lan, *Nat. Commun.*, 2016, **7**, 11204.

9 L. Liao, S. Wang, J. Xiao, X. Bian, Y. Zhang, M. D. Scanlon, X. Hu, Y. Tang, B. Liu

and H. H. Girault, *Energy Environ. Sci.*, 2014, **7**, 387-392.

10 W. F. Chen, C. H. Wang, K. Sasaki, N. Marinkovic, W. Xu, J. T. Muckerman, Y. Zhu and R. R. Adzic, *Energy Environ. Sci.*, 2013, **6**, 943-951.

11 W. Cui, N. Cheng, Q. Liu, C. Ge, A. M. Asiri and X. Sun, *ACS Catal.*, 2014, **4**, 2658-2661.

12 D. H. Youn, S. Han, J. Y. Kim, H. Park, S. H. Choi and J. S. Lee, *ACS Nano*, 2014, **8**, 5164-5173.

13 H. B. Wu, B. Y. Xia, L. Yu, X. Y. Yu and X. W. Lou, *Nat. Commun.*, 2015, **6**, 6512.

14 C. He and J. Tao, *Chem. Commun.*, 2015, **51**, 8323-8325.

15 Y. Zhao, K. Kamiya, K. Hashimoto and S. Nakanishi, *J. Am. Chem. Soc.*, 2015, **137**, 110-113.

16 R. Ma, Y. Zhou, Y. Chen, P. Li, Q. Liu and J. Wang, *Angew. Chem. Int. Ed.*, 2015, **54**, 14723-14727.

17 X. Yang, X. Feng, H. Tan, H. Zang, X. Wang, Y. Wang, E. Wang and Y. Li, *J. Mater. Chem. A*, 2016, **4**, 3947-3954.

18 Y. Liu, G. Yu, G. D. Li, Y. Sun, T. Asefa, W. Chen and X. Zou, *Angew. Chem. Int. Ed.*, 2015, **54**, 10752-10757.

19 K. Zhang, Y. Zhao, D. Fu and Y. Chen, *J. Mater. Chem. A*, 2015, **3**, 5783-5788.

20 W.-F. Chen, S. Iyer, S. Iyer, K. Sasaki, C.-H. Wang, Y. Zhu, J. T. Muckerman and E. Fujita, *Energy Environ. Sci.*, 2013, **6**, 1818-1826.

21 F. X. Ma, H. B. Wu, B. Y. Xia, C. Y. Xu and X. W. Lou, *Angew. Chem. Int. Ed.*, 2015, **54**, 15395-15399.

22 P. Xiao, Y. Yan, X. Ge, Z. Liu, J.-Y. Wang and X. Wang, *Appl. Catal. B: Environ.*, 2014, **154-155**, 232-237.

23 H. Lin, N. Liu, Z. Shi, Y. Guo, Y. Tang and Q. Gao, *Adv. Funct. Mater.*, 2016, **26**, 5590-5598.

24 L. Ma, L. R. L. Ting, V. Molinari, C. Giordano and B. S. Yeo, *J. Mater. Chem. A*, 2015, **3**, 8361-8368.

25 H. Vrubel and X. Hu, *Angew. Chem. Int. Ed.*, 2012, **124**, 12875-12878.

26 X. Fan, H. Zhou and X. Guo, *ACS Nano*, 2015, **9**, 5125-5134.

27 J. Tian, Q. Liu, A. M. Asiri and X. Sun, *J. Am. Chem. Soc.*, 2014, **136**, 7587-7590.

28 Y. Liang, Q. Liu, A. M. Asiri, X. Sun and Y. Luo, *ACS Catal.*, 2014, **4**, 4065-4069.

29 S. Wang, J. Wang, M. Zhu, X. Bao, B. Xiao, D. Su, H. Li and Y. Wang, *J. Am. Chem. Soc.*, 2015, **137**, 15753-15759.

30 H. Fei, Y. Yang, Z. Peng, G. Ruan, Q. Zhong, L. Li, E. L. Samuel and J. M. Tour, *ACS Appl. Mater. Interfaces* , 2015, **7**, 8083-8087.

31 J. Shi, Z. Pu, Q. Liu, A. M. Asiri, J. Hu and X. Sun, *Electrochimica Acta*, 2015, **154**, 345-351.

32 X. Zou, X. Huang, A. Goswami, R. Silva, B. R. Sathe, E. Mikmeková and T. Asefa, *Angew. Chem. Int. Ed.*, 2014, **126**, 4461-4465.

33 C. Tang, Z. Pu, Q. Liu, A. M. Asiri and X. Sun, *Electrochimica Acta*, 2015, **153**, 508-514.

34 P. Jiang, Q. Liu and X. Sun, *Nanoscale*, 2014, **6**, 13440-13445.

35 Y. Zheng, Y. Jiao, L. H. Li, T. Xing, Y. Chen, M. Jaroniec and S. Z. Qiao, *ACS Nano*,

2014, **8**, 5290-5296.